Perturbation and adjoint analyses of flow-acoustic interactions in an unsteady 2D jet

By L. I. Cerviño†, T. R. Bewley†, J. B. Freund‡, AND S. K. Lele

It is well known that noise sources embedded in a jet produce sound fields which refract due to the presence of the flow. The refraction due to the mean flow has been appreciated and modeled for some time, but only occasionally is the significant refractive effect of the unsteadiness of the flow acknowledged. In the present work, perturbation and adjoint analyses of high-frequency acoustic fluctuations are performed in a numerical simulation of a cold 2D jet system at a Mach number of $M = 0.5$ and a Reynolds number based on the jet diameter of $Re_D = 5000$. The jet system is hydrodynamically excited into a sinuous mode near the jet exit at a Strouhal number of $St = 0.4$, and exhibits the classical vortex roll-up phenomenon. Acoustic perturbations to this flow system are analyzed at Strouhal numbers of $St = 0.8$, $St = 2$, and $St = 8$ (that is, 2×, 5×, and 20× the vortex roll-up frequency). It is found that the unsteady effects of the flow cause a significant frequency broadening in both the perturbation and adjoint analyses.

1. Introduction

The problem of jet noise has significant engineering consequences. The far-field noise radiated by an unsteady flow system may be computed directly from a highly-accurate simulation of the compressible Navier-Stokes equation, or may be extracted from an approximate compressible flow simulation using any of several "acoustic analogies", including the celebrated Lighthill and Lilley equations. Despite their elegance and the fact that they are exact expressions, such acoustic analogies generally fail to isolate the true "sources" of far-field noise from significantly stronger noise "sources" which almost completely destructively interfere and radiate relatively little energy to the far field, as with the so-called quadrupole noise sources in a turbulent jet.

In order to better understand the physics of far-field noise and how it may be controlled, the present investigation represents one in a series of efforts to interrogate numerical databases, which capture the production of far-field sound directly, by accurate simulations of the compressible Navier-Stokes equation. The present paper focuses on the significance of acoustic scattering due to unsteady vortex roll-up in the perturbation and adjoint analyses central to this investigation.

There have been several previous investigations aimed at analyzing the effects of refraction in perturbation and adjoint analyses due to the presence of the flow. Many of them, however, consider the governing equations only after they have been linearized about the mean flow. For example, Durbin (1983a, 1983b) derived a high-frequency Green's function from an idealized steady jet profile. Tam & Auriault (1998) obtained an adjoint Green's function, using a steady jet profile obtained from a RANS calculation, and related it to the corresponding Green's function of the acoustic field at a particular point in the flow field due to additional localized sources embedded within the jet.

† Univ. of California, San Diego
‡ Univ. of Illinois, Urbana-Champaign

In a turbulent flow, however, acoustic phenomena are closely related to system unsteadiness. This was characterized in Freund & Fleischman (2001), where a refraction analysis was performed by means of ray tracing. It was observed that, when a noise source was located within the laminar jet core, the difference in the directivity calculated by the mean flow analysis and the unsteady flow analysis was rather small. However, when the source was placed farther downstream on the jet axis, the rays in the mean flow were significantly refracted by the unsteady jet shear layers, and the time average of the unsteady analysis was completely different than the corresponding analysis of the mean flow. Suzuki & Lele (1999) and Suzuki (2001) performed Green's function analyses in unsteady 2D mixing layers and boundary layers and analyzed the effects of acoustic scattering. The interaction between incoming plane waves at various angles of incidence with the unsteady vortices in the flows were investigated in detail, and the results compared with the ray-tracing procedure. A significant broadening of the frequency content of the acoustic wave after it passed through the mixing layer was observed, indicating significant flow-acoustic interaction. The present paper extends these lines of investigation with perturbation and adjoint analyses of cold 2D jets.

1.1. *Approach*

As mentioned in the Abstract, the flow system considered in this work is a Mach 0.5 cold 2D jet at a Reynolds number $Re_D = \rho D U_j/\mu = 5000$ with sinusoidal excitation near the jet exit at $S_t = f_0 D/U_j = 0.4$. Refraction effects are expected to be significantly weaker in a cold jet than in a hot jet, as the speed of sound is identical in the ambient fluid and the jet core. In fact, in sharp contrast with the perturbation and adjoint analyses of the mean of a heated jet as considered by Tam & Auriault (1998), the corresponding analyses of the refraction due to the mean of the cold jet flow studied here exhibit very little refraction. Nevertheless, as shown in this paper, the acoustic scattering due to the unsteady vortex roll-up in the present flow is quite pronounced even in this cold jet system, illustrating significant opportunities to force the hydrodynamic field (at low frequencies) in order to modify the high-frequency radiated noise.

The simulation code used in the present work implements the full compressible Navier-Stokes equation using a numerical method based closely on that developed by Freund, Moin, & Lele (1997). The present simulations do not resolve any solid boundaries. Instead, artificial "buffer zones" have been used around the domain of physical interest, coupled with characteristic-based boundary conditions on the computational boundaries. This type of *ad hoc* but effective numerical boundary conditions simulates the effect of quiescent far-field boundary conditions on the physical system, and has now become standard for this type of problem. It is discussed further in, e.g., Freund (1997) and Colonius, Lele, & Moin (1993).

As summarized in Figure 1, two types of analyses are considered in the present work. In sec. 2, perturbation analyses of the flow field are performed in order to obtain a characterization of the propagation of disturbances in the system as it evolves forward in time. In these analyses, artificial RHS forcing (to be referred to in this paper as the "control") is introduced into the jet system, and the resulting perturbation to the flow which is introduced by this forcing is computed. As depicted in Figure 1, such analyses characterize **control→effect** relationships. A representative perturbation analysis of the present system is shown in the top row of Figure 2.

In sec. 3, adjoint analyses of the flow field are performed in order to characterize the sensitivity of a particular metric measuring the flow system to additional forcing of the governing equations. In these analyses, an "adjoint system" is defined and computed in

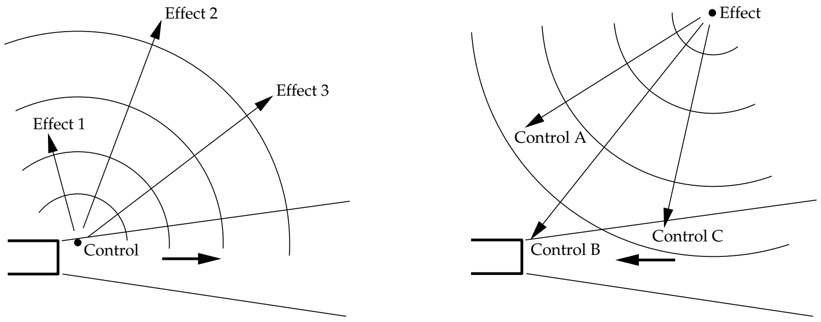

FIGURE 1. Perturbation analysis (left) and adjoint analysis (right) of the jet system.
Note that **perturbation analyses** characterize **control** $\rightarrow$ **effect** relationships:

- *If I change the "control" here, how and where will that affect the flow?*

On the other hand, **adjoint analyses** characterize **effect** $\rightarrow$ **control** relationships:

- *If I want to achieve a desired effect here, how and where should I apply "control" to the flow?*

The answer to the latter question is of particular interest when a high-dimensional forcing schedule for a complex system, such as a turbulent jet exhaust, is being optimized to achieve a desired effect, such as the reduction of radiated noise in a particular direction. Note that adjoint analyses do NOT identify the "source" of the radiated noise in such a system. Rather, they identify how and where additional forcing may be applied to the existing system to modify the radiating noise already present in a desired manner.

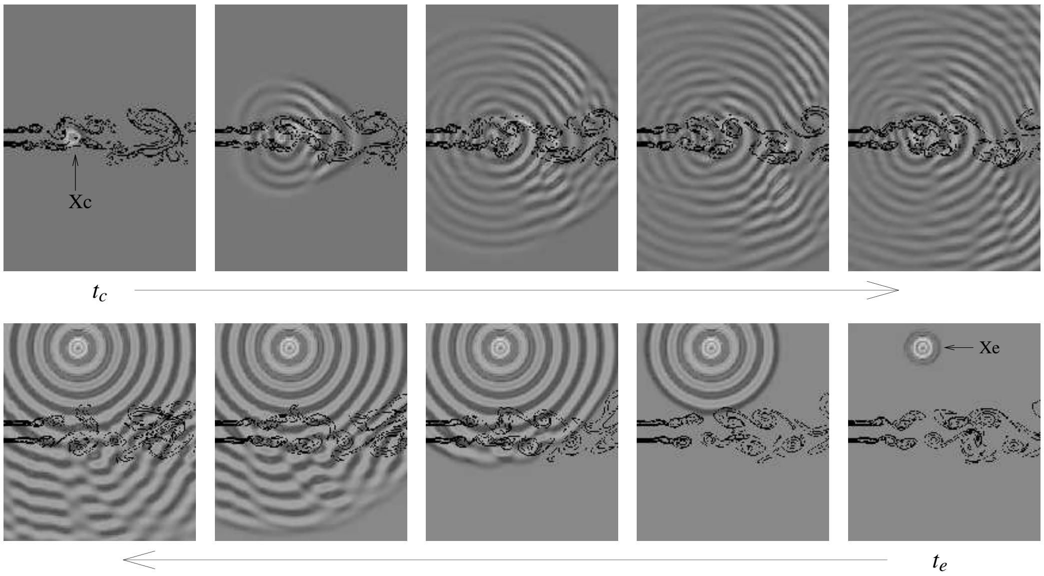

FIGURE 2. **Perturbation analysis** (top) characterizes the effect on the entire flow resulting from a small change to a particular "control" quantity, taken here to be a sinusoidally-varying mass source at point x_c. **Adjoint analysis** (bottom) characterizes the effect on a particular flow quantity, taken here to be high frequency noise at point x_e, due to small changes in the "control" applied anywhere in the flow. Note that a perturbation analysis involves marching the governing equation forward in time, whereas an adjoint analysis involves marching the corresponding adjoint equation backward in time.

order to identify the gradient of a "cost function" (which mathematically quantifies the metric of interest) to additional forcing of the jet system. As depicted in Figure 1, such analyses characterize **effect**$\rightarrow$**control** relationships. A representative adjoint analysis of the present system is depicted in the bottom row of Figure 2.

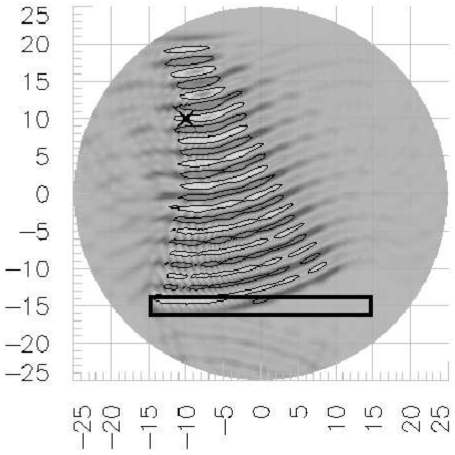

FIGURE 3. Adjoint analysis of sound waves, produced by a monopole sound source at the point marked by the X, in a stationary fluid. In the problem depicted here, the desired effect is to reduce the intensity of the sound field in the "interrogation region" outlined by the rectangular box. The corresponding adjoint field is driven by the sound waves in the box and propagates away from it, as visualized above, illustrating possible locations for "antinoise" sources where additional forcing could be applied to achieve the desired effect (namely, to reduce the sound pressure level within the box). Even though the governing system represented here is a linear, constant-coefficient PDE and the cost function is quadratic in the state variables, the adjoint field identifies a range of effective "antinoise" forcing locations, and does not accurately identify the isolated sound source. Note that the focusing of the adjoint field on the isolated sound source is found to improve when the size of the box is increased as compared with the wavelength of the sound.

It is important to note that adjoint analyses do *not* identify the "origin" or "source" of the radiated sound in such a system. This point is readily evident by considering a simpler model system (without the jet present), as depicted in Figure 3. Thus, identification of sound "sources" is not to be expected from adjoint analyses when applied to more complex systems, such as the unsteady jet considered in the present work.

Note that, in the remainder of the present work, the cost functions considered are essentially pointwise measures of the sound field, and the adjoint field computations are therefore referred to as "adjoint Green's functions".

2. Perturbation analyses

A logical starting place for this investigation is to assess the effects of hydrodynamic unsteadiness (that is, vortex roll-up) on small perturbations to the flow system. In particular, we will investigate the scattering of low-amplitude acoustic waves as they pass through the unsteady jet system. In order to perform a perturbation analysis of this sort, one approach is to calculate numerically the linearized ("perturbation") equations. The code used to solve such a problem is often referred to as a "tangent linear" code. With this approach, the perturbation field is obtained directly.

An alternative "finite-difference" approach allows us to calculate the perturbation field using the nonlinear flow solver itself, without writing a separate tangent linear code. This is achieved by computing a "nominal" flow, computing a second "perturbed" flow (with the appropriate small perturbation applied to the initial conditions, the boundary conditions, or the right-hand-side forcing), and taking their difference, dividing by the perturbation amplitude ε. In fact, in the $\varepsilon \to 0$ limit, this is how we define the so-called "perturbation field". However, as a computational strategy, this approach presents certain difficulties. If ε is made too small, the finite-precision arithmetic of the computer leads to differencing errors, as the two fields being compared are almost identical. On the other hand, if ε is made too large, the "small" perturbation assumption breaks down, and ε^2 terms in the Taylor series expansion begin to become significant. In practice, selecting an appropriate value of ε to minimize the sum of these spurious effects is difficult. Though higher-order finite-difference approximations of the perturbation field can be proposed, they are also plagued by the competition of these two spurious effects.

In order to circumvent the difficulties cited above associated with selecting ε in a finite-difference approximation of the perturbation field, an alternative approach, referred to as the Complex Step Derivative (CSD) method, has been developed (Lyness & Moler (1967); Squire & Trapp (1998)). This method has already been applied broadly in the optimization literature (see, e.g., Martins, Sturdza, & Alonso (2001)). The basis of this method is to redefine all of the real variables in the system as complex, and to perform the nominal (real) simulation as before while introducing the small perturbation into the imaginary part of the system. It can be shown by a straightforward Taylor-series expansion of the complex fields which result that, to order ε^2, the real part of the resulting field contains the nominal flow and the imaginary part (divided by ε) contains the perturbation field sought. Further, this calculation is not plagued by the "difference of large numbers" problem, so ε may be made very small without inducing differencing errors in the calculation of the perturbation field. This provides an extremely accurate technique for computing a perturbation analysis when the simulation code nominally involves only real arithmetic (as is the case with the present 2D simulations), and is the approach selected in the present computations†.

The result of a representative perturbation analysis is shown in the top row of Figure 2. A localized mass source which oscillates sinusoidally in time (at five times the vortex roll-up frequency of the jet) has been introduced in the jet at point x_c. This has been accomplished by adding a forcing term to the right-hand side of the continuity equation. The addition of this forcing excites an acoustic wave, which is significantly refracted by the unsteady vortex roll-up. Mean-flow analyses, of course, fail to capture such scattering, which is due to the unsteadiness of the flow.

It is also straightforward to characterize acoustic waves coming from the far field. Computationally, the approach is slightly different: unsteady forcing is used along a line within the non-physical "buffer zone", and particular care must be exercised to avoid spurious effects in the corner regions of the computational domain. Physically, however, the result is qualitatively similar, and significant scattering is encountered when the acoustic field passes through the unsteady jet, as shown in Figure 4.

† In fact, it is interesting to note that it is straightforward to extend the CSD method to pseudospectral codes which nominally employ complex arithmetic. This approach was investigated briefly during the CTR summer program, and is reported in Cerviño & Bewley (2002). Unfortunately, the FFT's used in such pseudospectral extensions of the CSD approach combine the nominal (real) and perturbation (imaginary) parts of the analysis, and thus the accuracy of this approach for computing the perturbation field is found to be not significantly better than the second-order finite-difference approach.

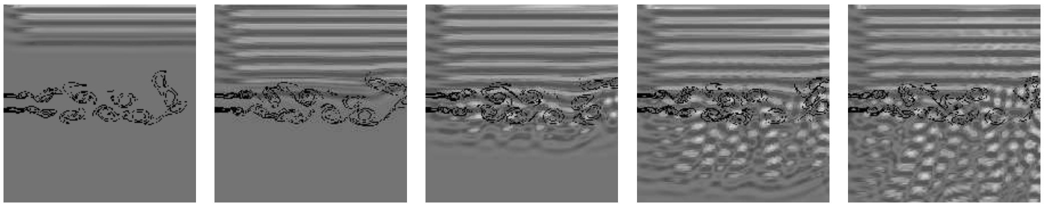

FIGURE 4. Perturbation analysis: refraction of pressure waves coming from the far-field by the unsteady 2D jet system

3. Adjoint analyses

The ultimate goal of the present research effort is to identify effective control strategies to reduce appropriate metrics of jet noise, extending the previous work reported by Wei & Freund (2002) of reducing the noise in a 2D mixing layer using a similar adjoint-based approach. Thus, though the perturbation analyses are qualitatively interesting, adjoint analyses contain significantly more relevant quantitative information related to our ultimate goal, and form the focus of the remainder of this study.

3.1. *The adjoint operator*

We now summarize briefly the adjoint formulation used in the present work. The continuous (PDE) description of the governing equation is first linearized and integrated by parts to obtain both an adjoint PDE operator useful in defining the adjoint field, and an identity that (once boundary conditions, initial conditions, and the right-hand-side forcing of the adjoint system are defined appropriately) may be used to express the required flow sensitivities in the continuous setting. As a final step before implementation in the numerical code, the state and adjoint equations are discretized in space and time in a consistent fashion.

We first define a state vector $\mathbf{q}$, a perturbation vector $\mathbf{q}'$, and adjoint vector $\mathbf{q}^*$ as

$$\mathbf{q} = \begin{pmatrix} p \\ \rho\mathbf{u} \\ \rho \end{pmatrix} = \begin{pmatrix} p \\ \mathbf{m} \\ \rho \end{pmatrix}, \qquad \mathbf{q}' = \begin{pmatrix} p' \\ \mathbf{m}' \\ \rho' \end{pmatrix}, \qquad \mathbf{q}^* = \begin{pmatrix} p^* \\ \mathbf{m}^* \\ \rho^* \end{pmatrix}. \tag{3.1}$$

We may then denote the nondimensionalized full compressible Navier-Stokes equation for an ideal gas with constant specific heats c_p and c_v and constant Prandtl number Pr as

$$\mathcal{N}(\mathbf{q}) = 0, \tag{3.2}$$

where

$$\mathcal{N}(\mathbf{q}) = \begin{pmatrix} \dfrac{\partial \rho}{\partial t} + \nabla\cdot\mathbf{m} \\ \dfrac{\partial \mathbf{m}}{\partial t} + \nabla\cdot\dfrac{\mathbf{m}\otimes\mathbf{m}}{\rho} + \nabla p - \dfrac{1}{Re}\nabla\cdot\left(\mu\nabla\dfrac{\mathbf{m}}{\rho}\right) - \dfrac{1}{Re}\nabla\left[\mu\left(\dfrac{\mu_B}{\mu}+\dfrac{1}{3}\right)\nabla\cdot\dfrac{\mathbf{m}}{\rho}\right] \\ \dfrac{\partial p}{\partial t} + \nabla\cdot\dfrac{p\mathbf{m}}{\rho} + (\gamma-1)\,p\left(\nabla\cdot\dfrac{\mathbf{m}}{\rho}\right) - \dfrac{\gamma}{Re\,Pr}\nabla\cdot\left(\mu\nabla\dfrac{p}{\rho}\right) - \Phi \end{pmatrix},$$

and Φ denotes the irreversible viscous dissipation term. Assuming appropriate expressions for μ and μ_B, the simulation code used in the present work implements the full compressible Navier-Stokes equation outlined above. In order to develop an adjoint solver, certain additional approximations have been made, namely that $\mu=$ constant, $\mu_B=$ constant, and $\Phi=0$. These convenient simplifications are thought to be acceptable in the approximate adjoint analysis, as the spatial and temporal variations of viscosity in the system and the irreversible viscous dissipation in the heat equation both affect the dynamics of the system only at the small length scales, and are thus thought to be relatively unimportant in terms of the mechanics of sound generation. Subject to these additional assumptions, and following the established procedure for performing an adjoint analysis [see, e.g., appendix B of Bewley, Moin, & Temam (2001) for the case of an unsteady compressible Euler system], we may take the Fréchet derivative of this governing equation to obtain a linearized equation of the form

$$\mathcal{N}'(\mathbf{q})\,\mathbf{q}'=0. \tag{3.3}$$

Selecting an L_2 duality pairing† of the form $\langle\mathbf{q}^*,\mathbf{q}'\rangle \triangleq \int_0^T\int_\Omega \mathbf{q}^*\cdot\mathbf{q}'\,d\mathbf{x}\,dt$, this linearized operator is then transformed according to the identity

$$\langle\mathbf{q}^*,\mathcal{N}'(\mathbf{q})\,\mathbf{q}'\rangle = \langle\mathcal{N}'(\mathbf{q})^*\,\mathbf{q}^*,\mathbf{q}'\rangle + b. \tag{3.4}$$

After some algebra involving several integrations by parts, it is straightforward to show that the adjoint operator corresponding to the approximate linearized form of the compressible Navier-Stokes equation in this framework is:

$$\mathcal{N}'(\mathbf{q})^*\,\mathbf{q}^* = \begin{pmatrix} -\dfrac{\partial\rho^*}{\partial t} - \dfrac{\mathbf{m}}{\rho}\cdot\nabla\rho^* + (\gamma-1)\,\rho^*\nabla\cdot\dfrac{\mathbf{m}}{\rho} - \nabla\cdot\mathbf{m}^* - \dfrac{\gamma\mu}{\rho\,Pr\,Re}\nabla^2\rho^* \\ -\dfrac{\partial\mathbf{m}^*}{\partial t} - \dfrac{\gamma p}{\rho}\nabla\rho^* - \dfrac{(\gamma-1)\rho^*}{\rho}\nabla p - \dfrac{\mathbf{m}}{\rho}\cdot\left(\nabla\otimes\mathbf{m}^* + (\nabla\otimes\mathbf{m}^*)^T\right) - \nabla p^* - \\ -\dfrac{\mu}{Re\,\rho}\left[\nabla^2\mathbf{m}^* + \left(\dfrac{\mu_B}{\mu}+\dfrac{1}{3}\right)\nabla(\nabla\cdot\mathbf{m}^*)\right] \\ -\dfrac{\partial p^*}{\partial t} + \dfrac{p\,\mathbf{m}}{\rho^2}\cdot\nabla\rho^* + \dfrac{(\gamma-1)\,\mathbf{m}}{\rho^2}\cdot\nabla(\rho^*\,p) + \dfrac{\mathbf{m}}{\rho}\cdot\left(\dfrac{\mathbf{m}}{\rho}\cdot\nabla\right)\mathbf{m}^* + \\ +\dfrac{\mu}{Re\,\rho^2}\left[\mathbf{m}\cdot\nabla^2\mathbf{m}^* + \left(\dfrac{\mu_B}{\mu}+\dfrac{1}{3}\right)(\mathbf{m}\cdot\nabla)(\nabla\cdot\mathbf{m}^*)\right] + \dfrac{\gamma\mu}{\rho\,Pr\,Re}\dfrac{p}{\rho}\nabla^2\rho^* \end{pmatrix}.$$

It is important to note that, in the present derivation, we have associated the "adjoint pressure" with additional forcing of the continuity equation, and the "adjoint density" with additional forcing of the selected form of the energy equation. [This is in contrast with, e.g., the nomenclature selected by Tam & Auriault (1998).] The nomenclature has been defined in this manner in order to have a logical zero-Mach-number limit. In this limit, ρ and ρ^* are constant, the forward and adjoint energy equations may be dropped, and the state, perturbation, and adjoint vectors reduce to

$$\mathbf{q}=\begin{pmatrix} p \\ \rho\mathbf{u}\end{pmatrix}=\begin{pmatrix} p \\ \mathbf{m}\end{pmatrix}, \qquad \mathbf{q}'=\begin{pmatrix} p' \\ \mathbf{m}'\end{pmatrix}, \qquad \mathbf{q}^*=\begin{pmatrix} p^* \\ \mathbf{m}^*\end{pmatrix}.$$

In a domain enclosed by solid boundaries, by selecting the appropriate adjoint boundary and initial conditions, we can make the boundary term b in (3.4), which results from the several integrations by parts, equal to zero. Alternatively, as in the present analysis,

† In multiscale PDE systems such as the present, the L_2 duality pairing is not necessarily the best choice for defining the adjoint operator, and incorporating spatial or temporal derivatives into this pairing is recognized to have an important regularizing effect on the spectra of the resulting adjoint field that must be calculated. For further discussion of this important topic, see Protas, Bewley, & Hagen (2002).

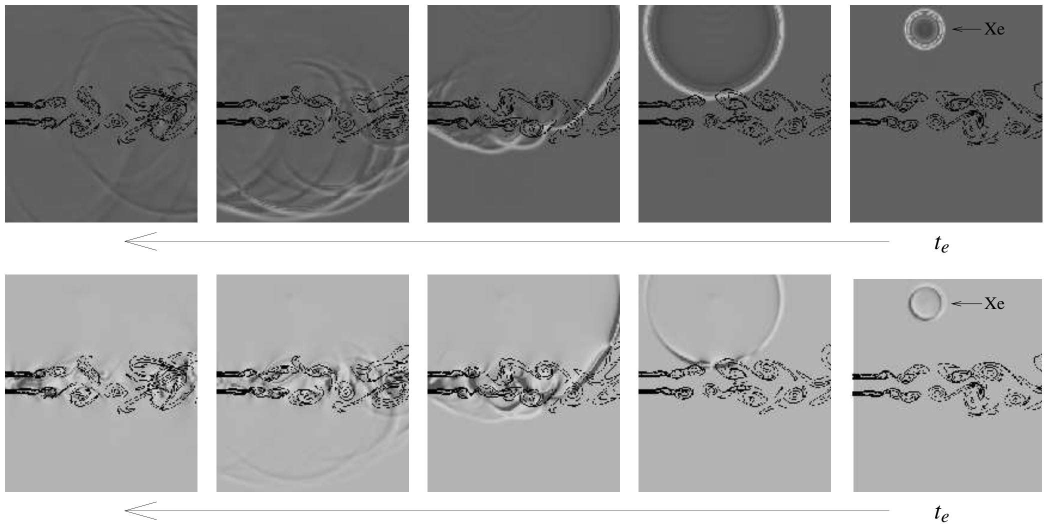

FIGURE 5. Adjoint density (top) and adjoint pressure (bottom) reveals sensitivity of the pressure component of the perturbation field at point x_e at time t_e to additional forcing of, respectively, the energy equation (top) and the continuity equation (bottom) everywhere in space x_c and for all times $t_c < t_e$. Note that, by causality, the adjoint field is zero for $t_c > t_e$; that is, the adjoint field marches backward in time from $t = t_e$.

we may surround the physical part of the domain of interest in both the flow and adjoint problems with the numerical equivalent of quiescent far-field boundary conditions which propagate no information towards the physical domain of interest; this again effectively allows us to neglect the influence of b. By so doing, the adjoint identity (3.4) then reveals that the following two analyses are equivalent:

#1) analyzing the effect on $q_i'(\mathbf{x}_e, t_e)$ (that is, the effect on the i'th component of the perturbation field at point $\mathbf{x} = \mathbf{x}_e$ and time $t = t_e$) created by applying a localized force $g_j' = \delta(\mathbf{x} - \mathbf{x}_c)\delta(t - t_c)$ to the j'th component of the perturbation equation, and

#2) analyzing the effect on $q_j^*(\mathbf{x}_c, t_c)$ created by applying a localized force $g_i^* = \delta(\mathbf{x} - \mathbf{x}_e)\delta(t - t_e)$ to the i'th component of the adjoint equation.

By the identity (3.4), we may relate the perturbation and adjoint fields in these two analyses by

$$q_i'(\mathbf{x}_e, t_e) = q_j^*(\mathbf{x}_c, t_c). \tag{3.5}$$

Note that the point $\mathbf{x}_c$ and time t_c do not appear in the formulation of the adjoint system in problem #2, but arise only in the subsequent analysis of the resulting adjoint field. Thus, a *single* adjoint calculation allows us to quantify the effect of forcing *anywhere* in the flow system (for any $\mathbf{x}_c$, t_c, and j) on the particular flow quantity $q_i'(\mathbf{x}_e, t_e)$. This relation between the perturbation and adjoint Green's functions provides an alternative but equivalent explanation of the significance of adjoint analyses to the more general "controls-oriented" explanation provided in Figure 1.

3.2. *Calculation of an adjoint Green's function*

Figure 5 illustrates a computation of the adjoint Green's function, as formulated at the end of the previous section, obtained by forcing the adjoint system $\mathcal{N}'(\mathbf{q})^* \mathbf{q}^* = \mathbf{g}^*$ with

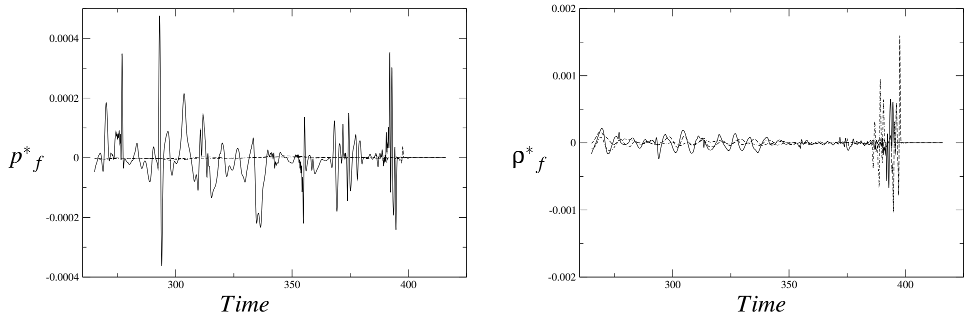

FIGURE 6. Evolution of adjoint pressure (left) and adjoint density (right) in time at the points $\{x, y\}$ of (solid) $\{5D, 0\}$, (dashed) $\{5D, 2.5D\}$, (dot-dashed) $\{5D, -2.5D\}$.

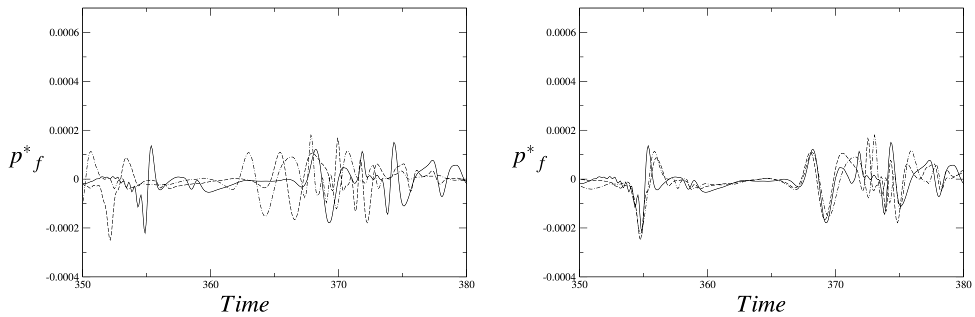

FIGURE 7. Adjoint pressure at three different locations at the centerline: at (dot-dashed) $x = 8$, (dashed) $x = 9$, and (solid) $x = 10$. When the actual evolutions of the variable (left) are shifted by the time corresponding to the convection velocity (right), there is an approximate superposition of the three lines, which indicates that these perturbations convect toward the nozzle at the convective speed.

an isolated force at a particular point in space and time, that is, $g_i^* = \delta(\mathbf{x} - \mathbf{x}_e)\delta(t - t_e)$. As discussed above, each component j of the resulting adjoint Green's function, at each point in space $\mathbf{x}_c$ and each instant in time t_c, may be interpreted as the i'th component of the perturbation to the flow at point $\mathbf{x}_e$ and time t_e that would arise due to localized forcing of the corresponding component j of the flow system at the corresponding point in space $\mathbf{x}_c$ and time t_c. The calculation reported in Figure 5 takes $i = 1$, that is, the adjoint field shown characterizes the effect on the perturbation pressure $p'(x_e, t_e)$.

It is interesting to note (see Figure 5) that the disturbance in the adjoint pressure grows rapidly as it propagates within the jet towards the nozzle at the convective velocity as the adjoint field evolves (in backwards time). In contrast, the disturbance in the adjoint density essentially propagates right through the jet, experiencing significant refraction. This behavior is quantified further in Figures 6 and 7. The component of the adjoint density that propagates at the convective speed of the jet within the jet shear layers is found to be quite small. This indicates, as one might expect, that mass sources are more efficient than energy sources in modifying the hydrodynamic field in a way which changes the radiated noise.

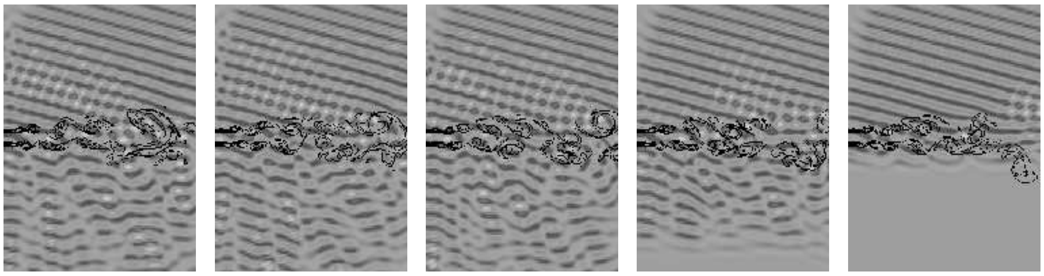

FIGURE 8. Adjoint density field due to incoming waves from the far field.

3.3. *An adjoint Green's function at temporal frequency f*

An alternative to forcing the adjoint problem at an isolated time t_e is to force it at a specific temporal frequency f. This corresponds roughly to looking at the sensitivity of the sound field at point x_e (at the frequency and phase selected) to additional forcing of the governing equations. This correspondence is only approximate, however, as the system under consideration has time-varying coefficients, and therefore frequency-based characterizations of the system's response are of limited usefulness. Note that, in systems with constant coefficients, a Bode plot completely characterizes the frequency response of the system. Such a frequency-domain analysis may only be applied to the mean flow. Nonetheless, an approximate characterization of this sort may still be developed for the present system (in the time domain) simply by forcing the adjoint system sinusoidally at the frequency of interest during the backwards march for the adjoint field. The result of such a calculation is illustrated in the bottom row of Figure 2. The scattering of the adjoint field due to the vortex roll-up is a necessary consequence of the scattering in the corresponding perturbation fields.

3.4. *An adjoint Green's function corresponding to far-field noise*

An alternative to forcing the adjoint problem at an isolated point in the computational domain x_e is to force it along a line near the boundary of the computational domain (that is, in the "buffer zone" used to approximate the far-field boundary conditions). By so doing, one may set up a propagating wave in the adjoint field which is the same as if the computational domain extended deep into the far field and the adjoint problem was forced a very long distance away. By varying the forcing along this line sinusoidally, one may simulate the arrival of a wave in the adjoint field corresponding to the effect on the far-field noise in any direction of interest. A representative example is given in Figure 8. Note that both reflection and refraction of the adjoint field are observed in this computation.

3.5. *Quantification of scattering of adjoint Green's functions*

In an attempt to quantify the scattering of a wave in the adjoint field due to the unsteady vortex roll-up, the values of the adjoint density and adjoint pressure have been measured at three different points in the representative adjoint Green's function analysis illustrated in Figure 9. The points where the adjoint density and adjoint pressure were measured are above the jet (where the scattering will be referred to as reflection), at the centerline, and below the jet (where the scattering will be referred to as refraction). The time series of these measurements were Fourier-transformed in time, and the results are plotted in Figure 10. The analysis was performed for adjoint forcing at three different Strouhal

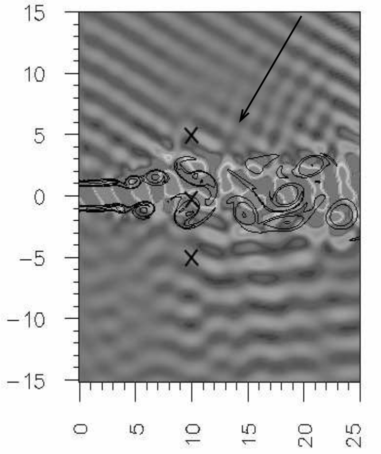

FIGURE 9. Adjoint pressure wave corresponding to far-field noise at an angle of 60° off the jet axis and at a frequency of $St = 2.0$. The Fourier transform of this field evaluated at the three points indicated is shown in Figure 10.

numbers: $St = 0.8$ (2× the vortex roll-up frequency), $St = 2.0$ (5× the vortex roll-up frequency), and $St = 8.0$ (20× the vortex roll-up frequency).

Perhaps the most important observation to make in Figure 10 is that there is very significant frequency broadening in all of the adjoint spectra measured. The adjoint systems are excited by forcing at the single frequency indicated ($St = 0.8$, 2.0, or 8.0) but, due to the time-varying coefficients (from the unsteady flow field $\mathbf{q}$) in the adjoint operator, the measurements of the adjoint field at the points indicated exhibit energy over a broad range of temporal frequencies. For comparison, the spectra of the hydrodynamic fluctuations of the base flow is shown in Figure 11. Note that the frequency broadening of the adjoint field cannot be captured by a steady-flow analysis.

The frequency broadening present when the adjoint field is forced at a high frequency is much larger than when it is forced at a low frequency. This fact was noticed by Suzuki (2001) for the direct problem, and was interpreted as "multiple scattering". In the present adjoint analysis, this suggests that high-frequency noise may be modified by a broad range of possible forcing frequencies.

Note in particular that the frequency spectrum is generally narrower at the point above the jet (dashed lines) than below the jet (dot-dashed lines), apparently because the refraction of the traveling wave in the adjoint field is stronger than the reflection of this wave for the incidence angle tested. Within the jet (solid line), it is observed that the frequency broadening is strongest.

The low-wavenumber components of the spectra of the adjoint pressure at the centerline are especially strong for all three forcing frequencies tested. This indicates that low-frequency modulation of the hydrodynamic field via mass sources within the jet can have a significant impact on the high-frequency noise in the far field, and provides impetus for further studies in jet-noise control based on such characterizations to exploit this sensitivity.

Note also that all of the spectra are somewhat jagged, and the distance between of each small peak in this jaggedness is $\Delta f = 0.2D/U$, which is exactly half of the vortex roll-up frequency. This appears to indicate (as one might expect) that the scattering of the wave in the adjoint field is closely related to its interactions with the large-scale vortex roll-up.

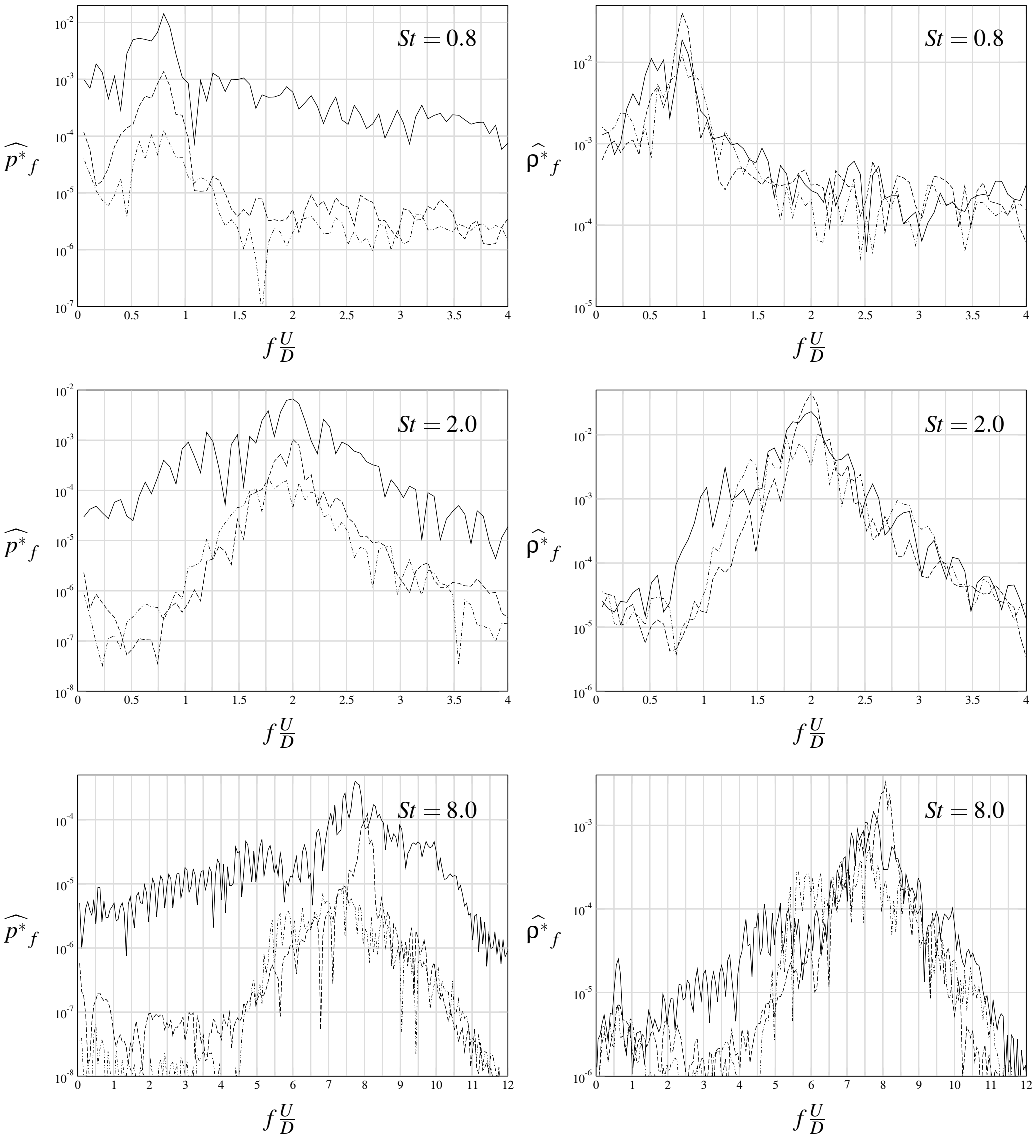

FIGURE 10. Temporal spectra of (left) the adjoint pressure $\widehat{p^*}_f$ and (right) the adjoint density $\widehat{\rho^*}_f$ for an incident wave in the adjoint field coming from above (at an angle of 60° off the jet axis), at a frequency of (top) $St = 0.8$, (middle) $St = 2.0$, and (bottom) $St = 8.0$ and measured at the points $\{x, y\}$ of (solid) $\{5D, 0\}$, (dashed) $\{5D, 2.5D\}$, (dot-dashed) $\{5D, -2.5D\}$. See Figure 9 for flow configuration.

A second set of cases was also run in which the wave in the adjoint field approaches the jet at a 90° angle off the jet axis (cf. Figure 9). The results showed very similar trends, and are thus not included here.

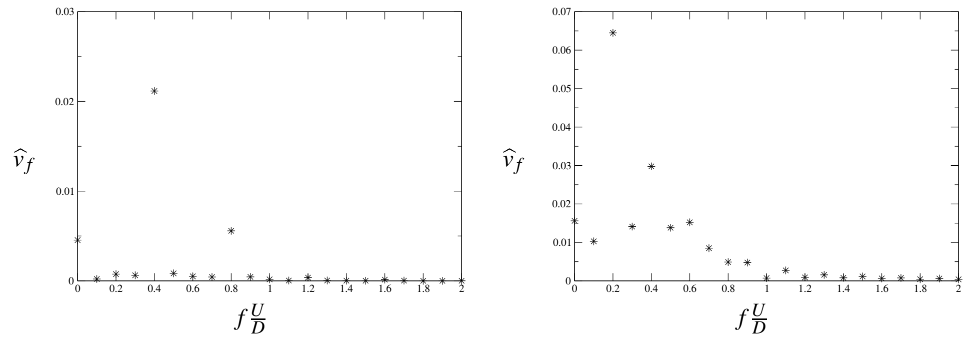

FIGURE 11. Spectra of the vertical velocity of the flow at $\{x,y\} = \{1.5D, 0.5D\}$ (left) and $\{x,y\} = \{3D, 0.5D\}$ (right). The appearance of the peak at $S_t = 0.2$ at the downstream station (right) is a result of vortex pairing (recall that the jet is forced at $S_t = 0.4$).

4. Concluding remarks

Perturbation and adjoint analyses of flow-acoustic interactions in an unsteady 2D jet have been performed. Attention has been focused on the scattering of adjoint Green's functions corresponding to far-field high-frequency noise. Significant scattering of the adjoint field is detected both above and below the jet, as quantified by a spectral analysis of the adjoint field. This scattering is a direct result of system unsteadiness (vortex roll-up), and cannot be captured by mean flow analyses.

The degree to which frequency broadening extends into the low frequencies within the jet in the adjoint analyses indicates the degree to which low-frequency alteration of the hydrodynamic field can be used to affect the high-frequency radiated acoustic field. This distinguishes promising low-frequency "hydrodynamic" control strategies from simple (but perhaps impractical) "antinoise" control strategies, which must be applied at the frequency of the radiated noise.

REFERENCES

BEWLEY, T.R., MOIN, P., & TEMAM, R. 2001 DNS-based predictive control of turbulence: an optimal benchmark for feedback algorithms. *J. Fluid Mech.* **447**, 179-225.

CERVIÑO, L.I. & BEWLEY, T.R. 2002 On the extension of the complex-step derivative technique to pseudospectral algorithms. Submitted for publication.

COLONIUS, T., LELE, S.K., & MOIN, P. 1993 Boundary conditions for direct computation of aerodynamic sound generation. *AIAA J.* **31**, 1574-1582.

DURBIN, P.A. 1983a High frequency Green function for aerodynamic noise in moving media, Part I: general theory. *J. Sound Vib.* **91**, 519-525.

DURBIN, P.A. 1983b High frequency Green function for aerodynamic noise in moving media, Part II: Noise from a spreading jet. *J. Sound Vib.* **91**, 527-538.

FREUND, J.B., MOIN, P., & LELE, S.K. 1997 Compressibility effects in a turbulent annular mixing layer. Mech. Engg. Dept., Stanford University, Tech. Rept. TF-72.

FREUND, J.B. 1997 Proposed inflow/outflow boundary condition for direct computation of aerodynamic sound. *AIAA J.* **35**, 740-742.

FREUND, J.B., & FLEISCHMAN, T.G. 2001 A numerical study of jet noise mechanisms: sound scattering by turbulence. *AIAA Paper* 2001-0375.

Lyness, J.N. & Moler, C.B. 1967 Numerical differentiation of analytic functions. *SIAM J. Numer. Anal.* **4**, 202-210.

Martins, J.R.R.A., Sturdza, P., & Alonso, J.J. 2001 The connection between the complex-step derivative approximation and algorithmic differentiation. *AIAA Paper* 2001-0921.

Protas, B., Bewley, T.R., & Hagen, G. 2002 A comprehensive framework for the regularization of adjoint analysis in multiscale PDE systems. Submitted.

Squire, W. & Trapp, G. 1998 Using complex variables to estimate derivatives of real functions. *SIAM Rev.* **40**, 110–112.

Suzuki, T., & Lele, S.K. 1999 Acoustic scattering from a mixing layer: role of instability waves. *AIAA Paper* 99-0228.

Suzuki, T. 2001 Acoustic wave propagation in transversely sheared flows. PhD Thesis, Stanford University, Department of Aeronautics and Astronautics. Also available as SUDAAR 739.

Tam, C.K.W. & Auriault, L. 1998 Mean flow refraction effects on sound radiated from localized sources in a jet. *J. Fluid Mech.* **370**, 149-174.

Wei, M. & Freund, J.B. 2002 Optimal control of free shear flow. *AIAA Paper* 2002-0665.